J. Fluid Mech. (1996), *vol.* 315, *pp.* 367–385

The motion of a solid sphere suspended by a Newtonian or viscoelastic jet

By J. FENG† AND D. D. JOSEPH

Department of Aerospace Engineering and Mechanics and the Minnesota Supercomputer Institute, University of Minnesota, Minneapolis, MN 55455, USA

(Received 28 December 1994 and in revised form 22 December 1995)

This paper describes experimental observations of a solid sphere suspended by a vertical or inclined jet. A laminar Newtonian jet is able to suspend a sphere only through viscous entrainment at low Reynolds numbers ($Re \sim 10$). A turbulent Newtonian jet ($Re \sim 10^4$) attracts a sphere that is sufficiently large but rejects smaller ones. The Coanda effect is responsible for steady suspension of solid spheres even in highly slanted jets. Anomalous rotation, opposite to the direction of the local shear, occurs under certain conditions, and its physical mechanism cannot be explained based on available information. A viscoelastic laminar jet is narrower than a comparable Newtonian one and it can suspend spheres at Reynolds numbers in the hundreds, precisely the Re range in which a Newtonian jet fails to suspend a sphere. It is suggested that the contrast between laminar Newtonian and viscoelastic jets may be related to a reversal in the pressure distribution on the surface of the sphere caused by non-Newtonian normal stresses. Flow visualization provides insights into the flow field in the jet and around the solid sphere.

1. Introduction

In 1870, Osborne Reynolds published a paper about the suspension of a ball on top of a vertical water jet in air. He noticed a remarkable phenomenon: when the ball is moved away from the centre of the jet, it always goes back. The lateral restoring thrust results from the fact that the water on the inner side of the ball tends to adhere to the solid surface and is not thrown out until it passes the top of the ball. A similar effect has been observed with submerged jets. The easiest demonstration is the suspension of a ping-pong ball by an air jet generated by a hair-dryer. The physical mechanism is identified as the Coanda effect, by which a jet tends to flow along the curved surface of a solid body that is partially inserted into the jet, and is deflected to the side of the body. The Coanda effect can be easily explained by potential flow theory (Lighthill 1945). The reduction of flow area caused by the protruding solid body creates a low pressure in the jet which bends the jet along the solid surface. Interestingly, another flow phenomenon is also known by the name of Coanda effect. A thin air jet otherwise tangential to a curved solid surface will bend and flow along the surface, sometimes covering a large turning angle without separation (Newman 1961). This is a viscous effect associated with the flow of the surrounding fluid entrained by the jet (Wille & Fernholz 1965; Bradshaw 1973).

Based on the above works, it is well understood why a sphere can be in stable

† Present address: Department of Chemical Engineering, University of California, Santa Barbara, CA 93106-5080, USA.

equilibrium suspended by a vertical jet. More puzzling phenomena, however, have been observed when a freely rotating sphere or circular cylinder is introduced into the shear layer of a wide jet. Goldshtik (1981, 1990) described an 'anomalous rotation' of the solid body (opposite to the local vorticity) that occurs within a narrow range of submersion depth. At the same time, the cylinder or sphere experiences a lateral force that pushes it away from the jet, in obvious contrast to the Coanda effect. A potential flow theory was developed to explain the anomalous rotation (Goldshtik 1981) which relies on the postulate that the circulation around the solid object be such that the maximum velocity on the solid contour is minimized. Unlike the Kutta–Zhukowskii condition, this postulate has not found its justification from theories of viscous flow. The true mechanism is evidently related to viscosity.

The present paper was inspired by Goldshtik's work and will describe experimental findings about the motion of a free sphere suspended by a vertical or inclined liquid jet. Newtonian and viscoelastic fluids are used. Some of the observations cannot be readily explained from our knowledge of fluid mechanics. These results raise questions about the effects of viscous shear on the motion of particles, which bear great relevance to multiphase flows, and about the effects of viscoelasticity in such complex flows.

2. Experimental setup and procedure

The observations were done within a test chamber made of Plexiglas. Its bottom is a 25.4 cm × 25.4 cm square and its height is 38.1 cm. The jet is introduced by a nozzle mounted on the bottom of the chamber; the opening on the bottom plate is 8.6 cm from one side wall and 16.8 cm from the other. The nozzle can rotate in the mid-plane of the chamber to generate inclined jets (figure 1). The top of the chamber is open and the liquid overflows into a receiving trough that leads it back to the main tank. The simple loop is driven by a sine-pump and the flow rate is calibrated by a catch-and-measure method using a stop watch and an accurate scale. The sphere is introduced into the jet from the free surface above using a pair of long tweezers. The storage tank holds up to 120 l of liquid, though 50 l is enough to maintain steady circulation in the loop.

In our experiments, nozzles of three different inner diameters were used: $D =$ 1.092 cm (the small nozzle), 2.0 cm (the medium nozzle) and 2.54 cm (the large nozzle). In operation, smaller nozzles are inserted into the large one and secured by sealant. The length of the nozzle inside the chamber is between 6.35 and 8.75 cm. Aluminium, stainless steel, ceramic, rubber and glass spheres of diameters between 1.11 and 3.18 cm are used. For spheres of different material the results are qualitatively the same, and data will be presented selectively. Four different fluids were used: water, pure glycerin, 88 wt % glycerin in water and 0.85 wt % polyethylene oxide (Polyox-WSR301 provided by Union Carbide) in distilled water. The density and viscosity of the three Newtonian fluids are listed in table 1. The properties of the polyox solution have to be specifically measured.

One basic concern in using polyox solutions in a large flow loop is mechanical degradation. The solution was prepared in a large tank with mild agitation; the mixing took 10 days to complete. The design of the sine-pump also helps minimize damage to the molecular structure of the polymer. Because the characteristic shear rate (the maximum velocity in the nozzle divided by its radius) can be as high as 300 s^{-1}, and there is strong extension in the circulation, degradation did occur in the experiments. Three samples of the polyox solution (A, B and C) were taken before, during and after the experiments. Their shear-viscosity and dynamic modulii were measured in a

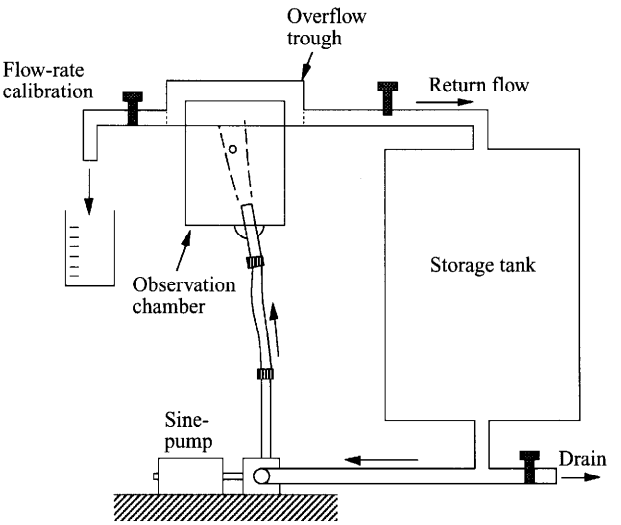

FIGURE 1. A schematic diagram of the flow loop and the observation chamber.

Fluids	Density ρ_f (g cm^{-3})	Kinematic viscosity ν (cm^2 s^{-1})
Water	0.998	0.01004
Pure glycerin	1.259	11.44
88 wt% glycerol	1.23	1.199

TABLE 1. The density and kinematic viscosity of the Newtonian test fluids at 20 °C

Rheometrics RFS-II rheometer (figure 2). The continuous degradation poses a difficulty for data reduction. We decided to use the viscosity curve of sample B in calculating the Reynolds number. The high-shear-rate portion of curve B in figure 2(*a*) is fitted to a power law:

$$\eta = 0.7859\dot{\gamma}^{-0.4465},$$

the units of η and $\dot{\gamma}$ being Pa s and s^{-1}, respectively. The characteristic shear rate lies well within the power-law range in all experiments. The density of the polyox solution is almost exactly the same as that of water.

The position of the suspended sphere is measured, without parallax errors, by two coordinate systems laid out on the front and back walls of the chamber. The angular velocity is determined from analysing a high-speed video recording of the sphere. Visualization has been done by two different methods. To show the outline of the entire flow-field, we first establish a steady circulation in the loop and then inject dye inside the storage tank. Pictures can be taken before the observation chamber receives too much of the coloured liquid. To show details of the flow near the sphere, we use a laser sheet to illuminate the symmetric plane of the flow. Tiny air bubbles naturally trapped in highly viscous liquids or generated in water by adding a small amount of detergent serve as tracers.

Because of the fragile nature of polyox solutions, the flow system has been designed to be simple and compact. A prudent researcher might be concerned with effects of the sidewalls on the jet or the disturbance of the pump to the flow. Also the continuous degradation throws doubt on the accuracy of the quantitative results. However, the data exhibit distinctive trends and should be reliable qualitatively.

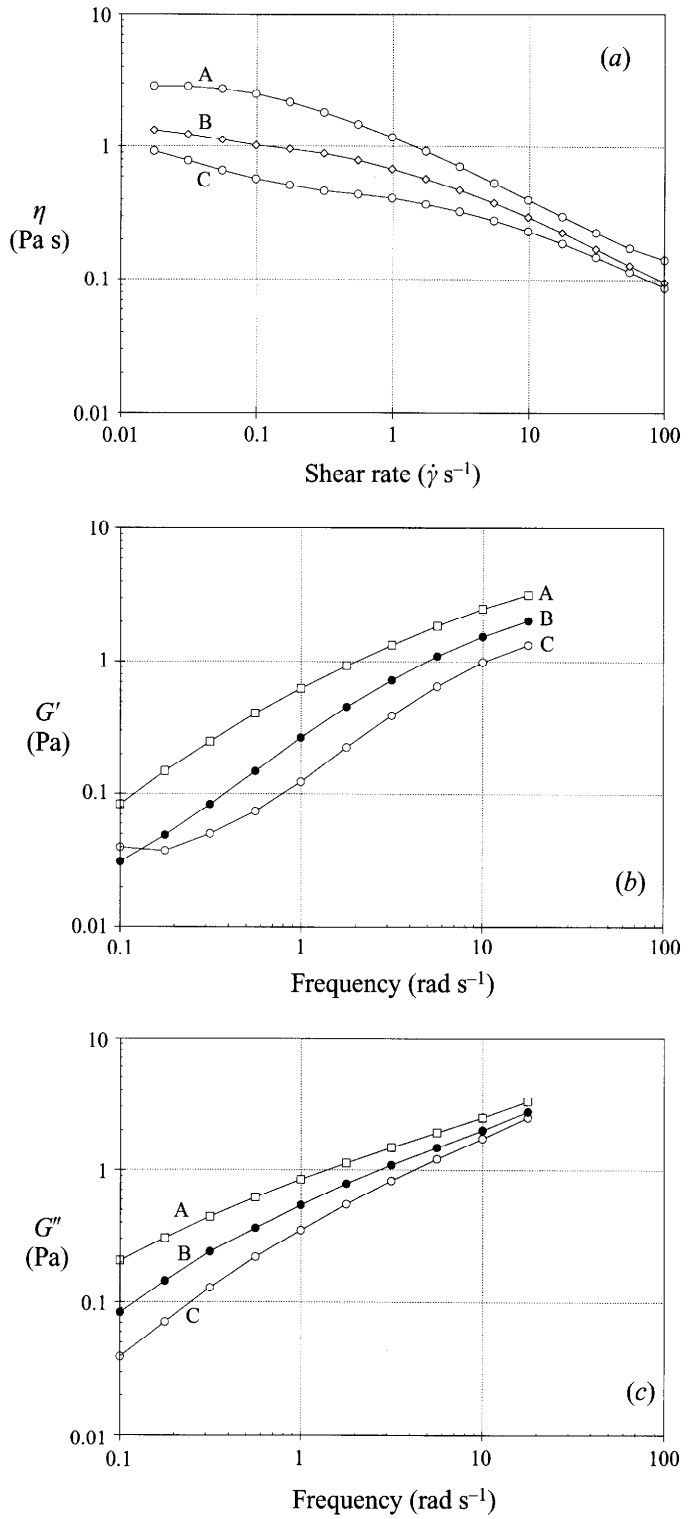

FIGURE 2. Degradation of 0.85 wt% polyox solution. Sample A was taken immediately after the solution was prepared; B was taken in the middle of the experiments and C after all experiments were finished. (*a*) Shear viscosity, (*b*) storage modulus and (*c*) loss modulus.

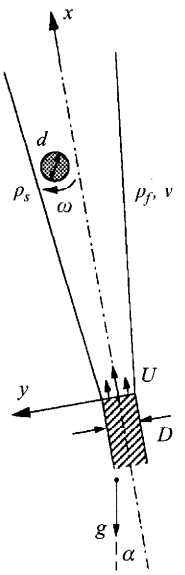

FIGURE 3. Flow parameters in an inclined Newtonian jet.

3. Results and discussion

3.1. *Newtonian jet*

In an inclined jet, a sphere cannot stay in the centre because of gravity. If there is a lateral force to support the sphere and ensure an eccentric equilibrium position for it (figure 3), then this position (x, y) and the rotation of the sphere ω depend on the following variables: the diameter and density of the sphere d and ρ_s, the density and kinematic viscosity of the fluid ρ_f and ν, the characteristic velocity of the jet U (the average velocity in the nozzle), gravitational acceleration g, the inner diameter of the nozzle D and its angle of inclination α. Dimensional analysis gives five independent dimensionless groups: $\rho = \rho_s/\rho_f$, $\kappa = d/D$, $Re = Ud/\nu$ (Reynolds number), $Fr = gd/U^2$ (Froude number) and α. These determine three dependent groups: $\Omega = \omega d/U$, x/D and y/D. We found that it is more convenient to combine Re, Fr and κ into another parameter $G = gD^3/\nu^2$. If we use G in place of Fr, the effect of U appears in Re only. Then for a set of experiments done with the same α, D and the same fluid, the only independent variables are Re and κ. Most of the data will be presented in terms of these parameters.

A submerged jet in a cylindrical vessel has four regimes of flow depending on the jet Reynolds number $Re_D = UD/\nu$ (McNaughton & Sinclair 1966): dissipated-laminar jet, fully laminar jet, semi-turbulent jet and fully turbulent jet. In our setup, the top of the chamber is left open and a dissipated-laminar jet never occurs. Even at the lowest Reynolds number, the jet was able to rise to the free surface. Interesting behaviour of a solid sphere has been observed in fully laminar and fully turbulent jets; this will be discussed in three distinctive ranges of the Reynolds number. Note that Re and Re_D are different but of the same order of magnitude.

3.1.1. *Low Reynolds numbers*

Those experiments were carried out using pure glycerin. The Reynolds number is of the order of 10 and the jet is laminar. At such low Re, the potential flow theory of Lighthill (1945) does not apply and it is impossible to have the sphere stably suspended

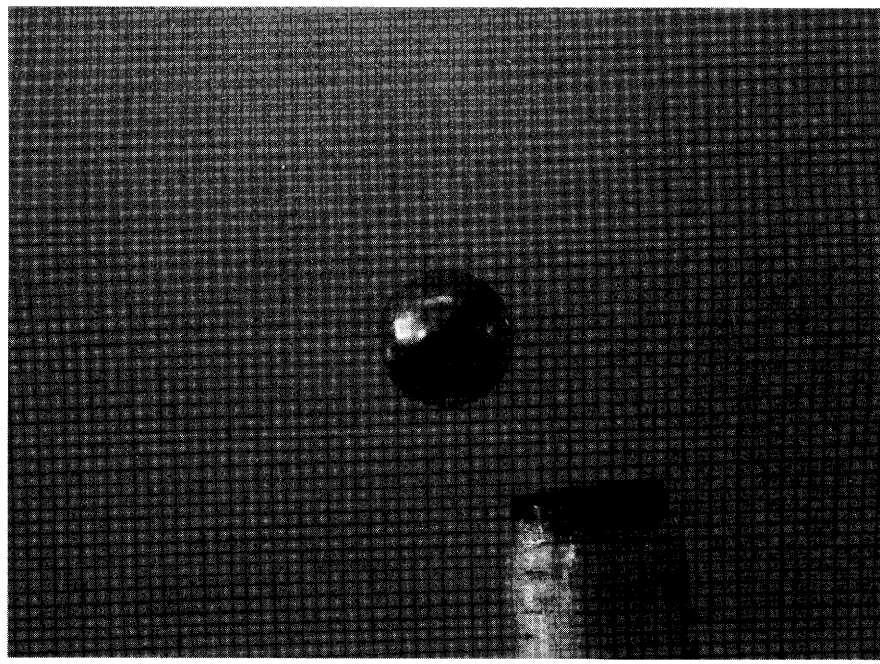

FIGURE 4. An aluminium sphere suspended by entrained flow outside of a Newtonian jet. $\rho = 2.755$, $\alpha = 4°$, $\kappa = 0.9525$, $Re = 11.59$, $G = 59.95$.

inside the jet. When placed on the centreline of a vertical jet, the sphere immediately jumps outwards and falls off.

However, if the sphere is carefully placed outside the mainstream near the exit, a stable suspension is possible. The sphere rotates steadily in the sense of the local shear (normal rotation). This equilibrium persists even if the nozzle is inclined up to a certain angle. Figure 4 shows a steadily spinning aluminium sphere suspended 'outside' the jet. The suspending force obviously comes from the flow of surrounding liquid that is entrained by the jet. Owing to the high viscosity of glycerin, the entrainment is very strong (Schlichting 1979, p. 233). The direction of the entrained flow is such that it creates a lateral force toward the centre of the jet in addition to the upward thrust. It is interesting to note that the steady suspension only exists within a specific range of Re. The sphere's position and angular velocity in this range are shown in figure 5 for a slightly inclined jet. As Re increases, the sphere moves up and slightly away from the centre of the jet and its rotation decreases. If Re exceeds the upper bound of the stable range, the sphere will first be pushed into the mainstream of the jet, where it is immediately thrown upwards. Then it is driven out of the jet at a high elevation and falls down. When it is close to the mouth of the nozzle, entrained flow again pushes it into the jet and the cycle is repeated. The amplitude of this oscillation increases with Re. If Re is reduced below the lower bound of the stable range, the sphere acquires a high-frequency, small-amplitude vibration. It eventually falls down if Re is further reduced.

3.1.2. *Medium Reynolds numbers*

These observations were made using 88 wt% glycerol. The Reynolds number is between 40 and 400, and the jet remains fully laminar. For all values of the parameters Re, G, α, κ and ρ that we can achieve, the sphere cannot be suspended by the jet, neither by the central part issuing from the nozzle nor by the entrained flow. If we hold a

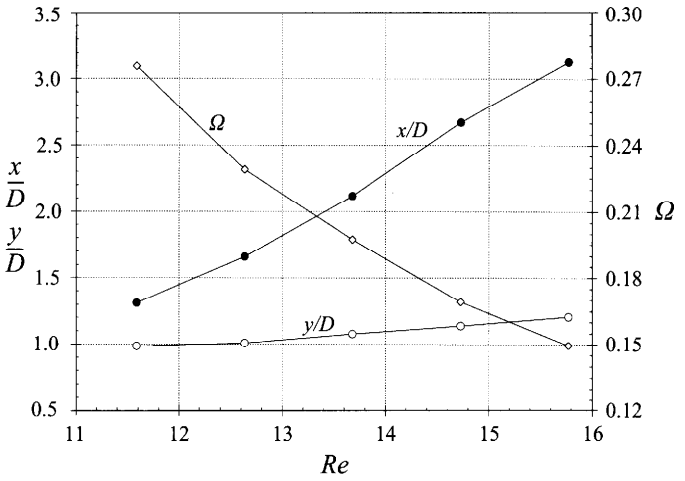

FIGURE 5. The position and rotation of an aluminium sphere suspended by entrained flow at low Reynolds number. $\rho = 2.755$, $\kappa = 0.9525$, $\alpha = 4°$, $G = 59.95$.

sphere in an eccentric position in the jet, we can feel a strong lateral thrust that pushes the sphere outwards. The mechanism of this lateral lateral repulsion may be related to the effects of the curvature of the velocity profile.

As an example, the range of *Re* covered using the medium nozzle and aluminium spheres of different diameters is between 44.4 and 130.4. It appears that the Reynolds numbers in this range are too small for the Coanda effect to be important, yet large enough that the viscous entrainment is severely suppressed. An important purpose of testing Newtonian jets in this *Re* range is for comparison with the viscoelastic polyox solution (§3.2). The concentration of glycerol was chosen such that its viscosity roughly matches that of the polyox solution under typical shear rates found in the experiment. We note in passing that the jet Reynolds number in our experiment is well within the laminar range of McNaughton & Sinclair (1966) but far exceeds the critical Reynolds number for a free jet (see, for example, Morris 1976). This is obviously a manifestation of the stabilizing effects of the sidewalls.

3.1.3. *High Reynolds numbers*

Using water as the test fluid, we obtained Reynolds numbers of the order of 10^4. The jet is fully turbulent (McNaughton & Sinclair 1966). For a vertical jet, steady suspension can be achieved within a range of flow rate as long as the sphere is larger than a critical size. Smaller spheres fall out of the jet at any flow rate. The smallest κ-value for which steady suspension was observed in our experiment is 0.675 (a 1.35 cm diameter aluminium sphere with the medium tube). The existence of a minimum κ was also reported by Goldshtik (1990), although he asserted that suspension is possible only if $d \geqslant D$. The flow rate has to be sufficiently large, of course, to carry the buoyant weight of the sphere. As U increases, the equilibrium position moves up. After U exceeds a threshold value, the sphere starts to oscillate up and down endlessly.

If the jet is slanted, the sphere shifts outward to an equilibrium position below the centreline of the jet. At large angles of inclination, the sphere is so far from the centre of the jet that it seems to be hanging onto the edge of the jet. As inclination increases, the range of flow rate for steady suspension narrows. For the largest inclination allowed by our device ($\alpha = 30°$), steady suspension can still be obtained with some spheres. It is easy to imagine that a maximum α exists beyond which steady suspension

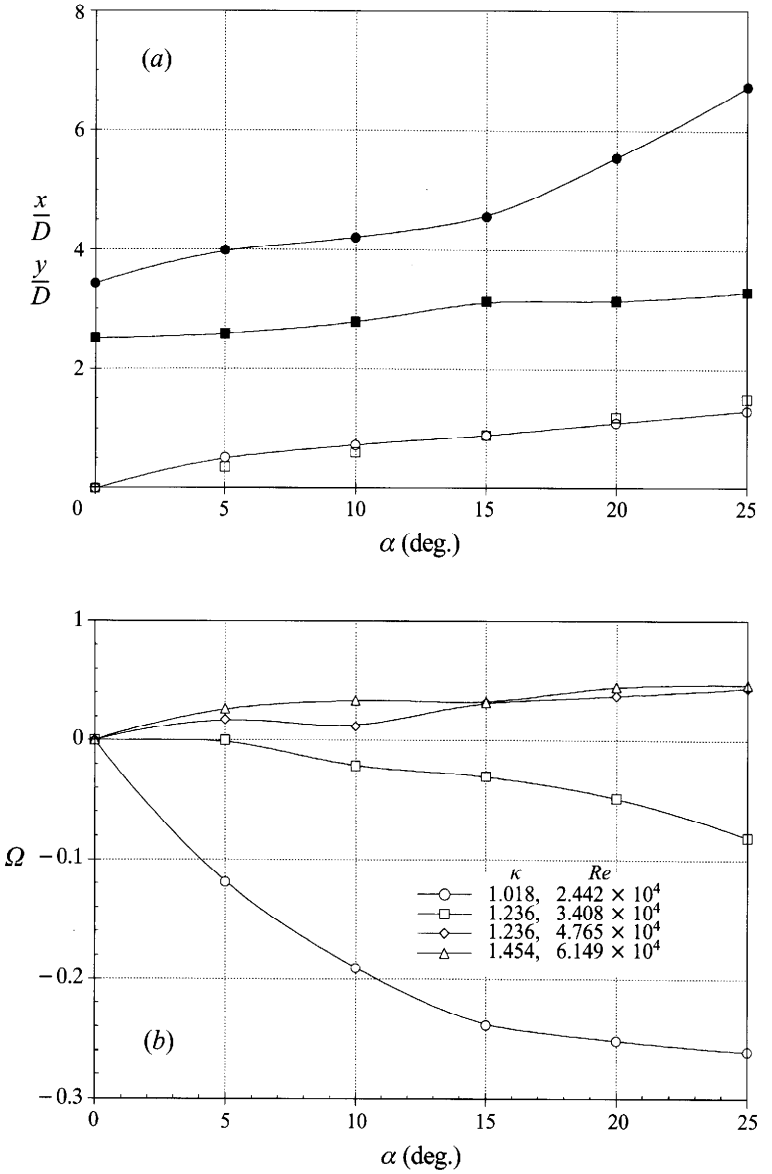

FIGURE 6. The position and angular velocity of stainless steel spheres at different inclinations of the jet issuing from the small nozzle. $\rho = 7.942$, $G = 1.227 \times 10^7$. (*a*) Position of two spheres. Filled symbols represent x/D and open ones y/D. Circle: $Re = 6.149 \times 10^4$, $\kappa = 1.454$; square: $Re = 2.442 \times 10^4$, $\kappa = 1.018$. (*b*) Angular velocities of three spheres at different Re.

is impossible. As soon as the jet is slanted, the sphere acquires a rotation that can be in either direction. Detailed data are presented next.

As mentioned earlier, we need only consider the effects of α, κ and Re for a fixed ρ and G. Using the same fluid, the same nozzle and spheres of the same material, we observed the following trend. Larger spheres tend to rotate normally and smaller ones anomalously. A sphere that rotates normally at large Re may rotate anomalously at smaller Re. Rotation in either direction increases as α increases.

The position and rotation as functions of α are illustrated in figure 6. As α increases, both x and y increase monotonically. This is because of the increasing component of

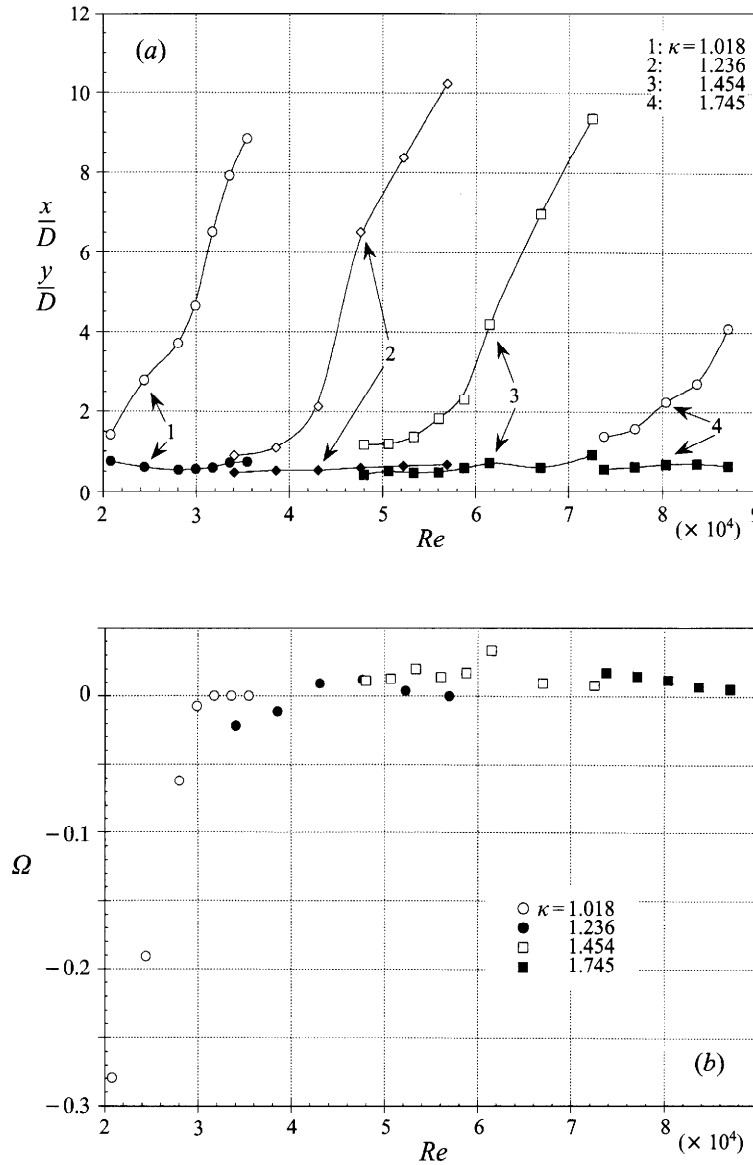

FIGURE 7. Position and rotation of stainless spheres with the small nozzle. $\rho = 7.942$, $G = 1.227 \times 10^7$, $\alpha = 10°$. (*a*) Position: open symbols represent x/D and filled ones y/D. (*b*) Angular velocity.

gravity in the y-direction and the decreasing component in the x-direction (cf. figure 3). The rotation, normal or anomalous, increases with α. The four curves in figure 6(*b*) also demonstrate the effects of κ and Re. Apparently, the effects of κ may be isolated by using a stronger jet for smaller spheres and thus keeping Re constant. But the spheres would end up at very different heights in the jet, and the difference in local shear would obscure the effects of κ. An alternative is to use spheres of different sizes but the same weight suspended at the same jet Reynolds number Re_D. This amounts to using a different combination of the independent variables in presenting the data.

For a fixed inclination $\alpha = 10°$, the effects of κ and Re on x/D, y/D and Ω have been studied using spheres of various materials and nozzles of different sizes. The trends are

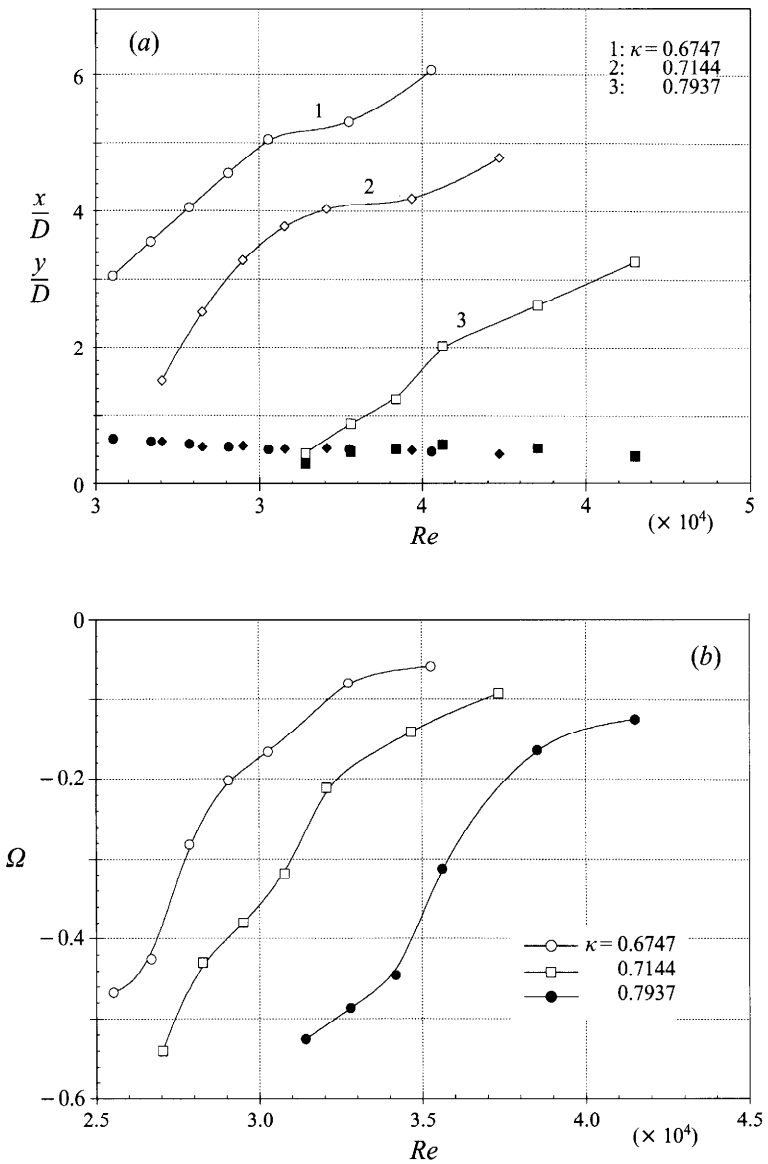

FIGURE 8. Position and rotation of stainless steel spheres with the medium nozzle. $\rho = 7.942$, $G = 7.848 \times 10^7$, $\alpha = 10°$. (*a*) Position: open symbols represent x/D and filled ones y/D. (*b*) Angular velocity.

the same in all runs. Figure 7 shows a typical set of results for stainless steel spheres with the small nozzle. With increasing flow rate (or *Re*), x/D increases monotonically (figure 7*a*). The variation in y/D is smaller and more susceptible to experimental errors. For normally rotating spheres, y/D increases with *Re* (curves 2, 3, 4). For anomalously rotating spheres, y/D tends to decrease with *Re* (curve 1). This is sometimes followed by a levelling off or even a slight increase as *Re* gets larger. This tendency appears consistently in all runs. The rotation of the sphere can be classified into three regimes. At small *Re* (below 4×10^4 in figure 7*b*), anomalous rotation prevails which decreases with *Re*. This may be associated with the fact that as the flow rate increases the sphere is driven higher and closer to the centre of the jet where it

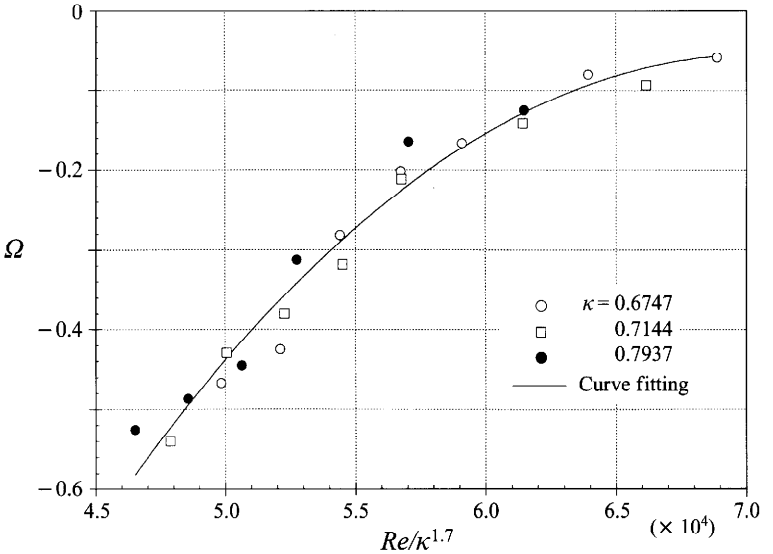

FIGURE 9. Correlation of the angular velocity of stainless steel spheres with the medium nozzle. $\rho = 7.942$, $G = 7.848 \times 10^7$, $\alpha = 10°$.

experiences smaller shear. The upper bound of this regime is where the sphere does not rotate at all. Further increasing *Re* induces an increasing normal rotation, which is the main feature of the second regime. In the third regime, increasing *Re* tends to reduce the speed of normal rotation. In this regime the sphere is floated in the upper part of the observation chamber where the jet is wide and the shear is relatively small.

A better picture of the first regime (with anomalous rotation) can be obtained using a larger nozzle (figure 8). Anomalous rotation prevails for the entire *Re*-range we can cover. Again y/D tends to decrease as *Re* increases. The most interesting feature of Ω is that curves with different κ are roughly 'parallel' to one another and can be collapsed onto one single curve by shifting *Re*. This gives rise to the 'master curve' in figure 9 which can be fitted into an empirical equation in terms of $Re\,\kappa^{-1.7}$:

$$\Omega = -4.644 + 1.305 \times 10^{-4}(Re\,\kappa^{-1.7}) - 9.279 \times 10^{-10}(Re\,\kappa^{-1.7})^2$$
$$\text{for} \quad \rho = 7.942, \quad G = 7.848 \times 10^7, \quad \alpha = 10°.$$

Data for aluminium spheres with the medium nozzle exhibit similar behaviour: a single curve can be obtained by plotting Ω against $(Re\,\kappa^{-1.57})$. The difference in the power index evidently reflects the effect of ρ. To show the effect of G, we go back to the results in figure 7(*b*). These data for stainless steel spheres with the small nozzle already appear to lie on a single curve, suggesting a small influence of κ. A better collapse is found using $Re\,\kappa^{-0.7}$ and the master curve can be fitted into the following formula (figure 10):

$$\Omega = 26.16 \exp(-1.071 \times 10^{-4}\, Re\,\kappa^{-0.7}) - 33.56 \exp(-1.145 \times 10^{-4}\, Re\,\kappa^{-0.7})$$
$$\text{for} \quad \rho = 7.942, \quad G = 1.227 \times 10^7, \quad \alpha = 10°).$$

The behaviour of suspended spheres raises a few questions. What is the flow mechanism of the jet–sphere attraction that keeps a ball in the centre of a vertical jet or hangs it on an inclined jet? What causes the anomalous rotation? As pointed out by Goldshtik (1990), the answer to the first question is the Coanda effect. Visualizations of the jet flow around normally and anomalously rotating spheres are shown in figure 11. For the thinner jet (figure 11*a*), there seem to be signs of the Coanda effect. The

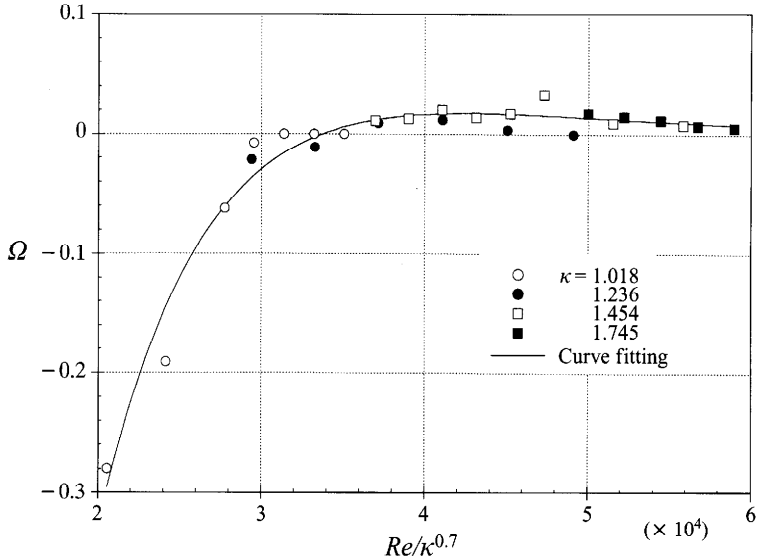

FIGURE 10. Correlation of the angular velocity of stainless steel spheres with the small nozzle. $\rho = 7.942$, $G = 1.227 \times 10^7$, $\alpha = 10°$.

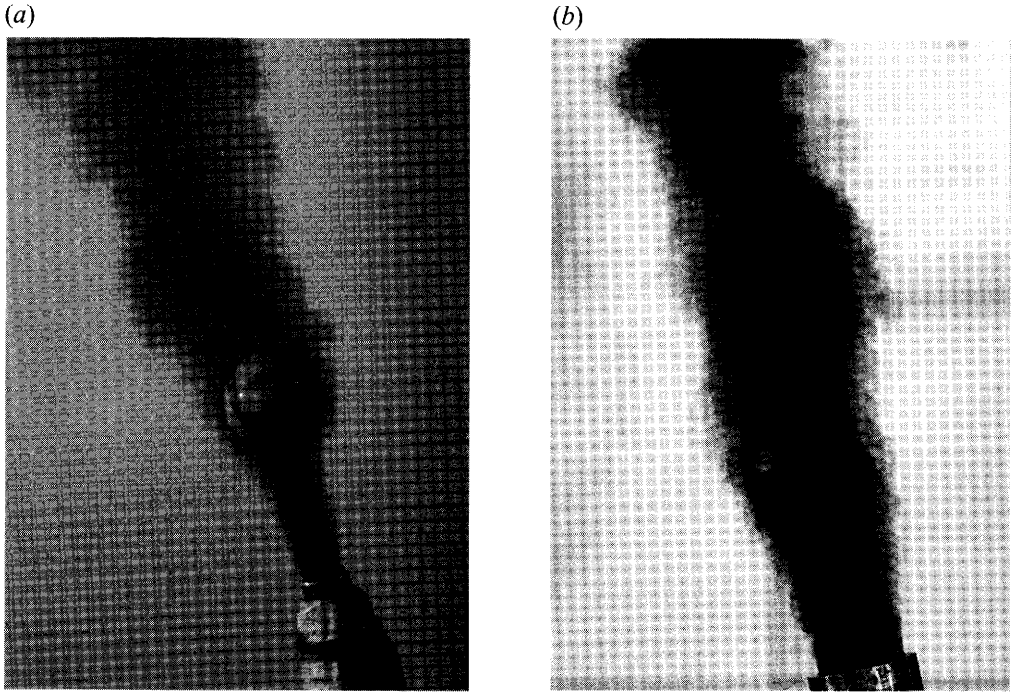

FIGURE 11. Flow around a sphere in an inclined jet. (*a*) Normal rotation of a ceramic sphere. $\rho = 3.813$, $G = 1.227 \times 10^7$, $\alpha = 12.5°$, $\kappa = 2.236$, $Re = 9.838 \times 10^4$, $(x/D,\ y/D) = (4.354,\ 0.8422)$ and $\Omega = 0.03857$. (*b*) Anomalous rotation of a rubber sphere. $\rho = 1.185$, $G = 1.608 \times 10^8$, $\alpha = 10°$, $\kappa = 1$, $Re = 1.652 \times 10^4$, $(x/D,\ y/D) = (3.174,\ 0.4387)$ and $\Omega = -0.2325$. One may note that the jet is deflected to the left (*a*) or the right (*b*) depending on the direction of rotation.

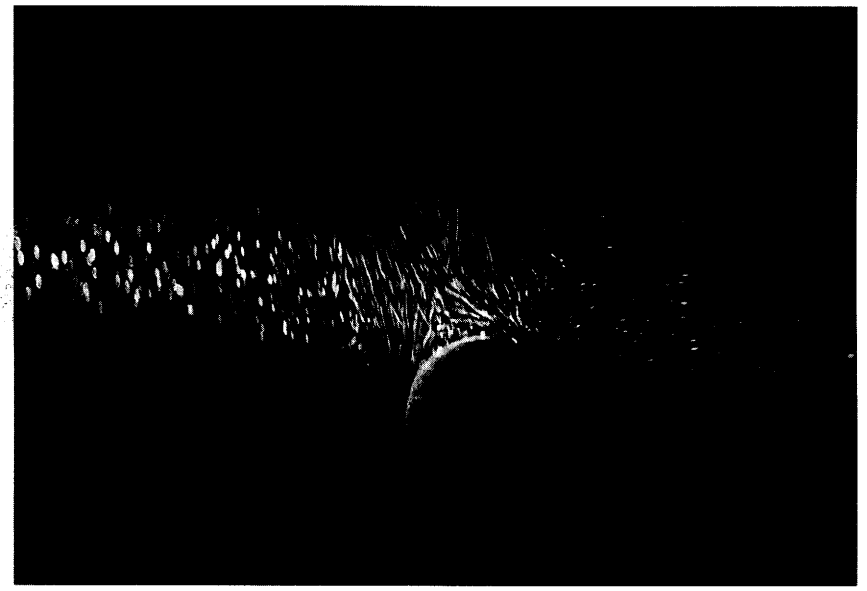

FIGURE 12. Visualization of the wake behind a non-rotating rubber sphere. The flow parameters are $\rho = 1.185$, $G = 7.848 \times 10^7$, $\alpha = 10°$, $\kappa = 1.27$, $Re = 1.906 \times 10^4$; the sphere is at $(x/D, y/D) = (1.99, 0.4295)$.

flow is more curved on the right-hand side of the ball; this flow wraps a larger portion of the solid surface and causes a bulge, after separation, on the upper left of the wake. For the thick jet in figure 11(*b*), no such signs are discernible. A better illustration of the Coanda effect comes from a closer image of the wake (figure 12). The flow conditions are such that the sphere is not rotating, and the wake is symmetric. The Reynolds number is 1.906×10^4 and there is a very small, if any, circulation zone behind the ball. In a uniform stream, the sphere would see a wide and long circulation zone behind it at such *Re* (Van Dyke 1982, p. 34). It is the jet's tendency to cling onto curved solid surfaces that explains the steady suspension of a sphere in a vertical or inclined jet. Note that the Coanda effect is a result of fluid inertia and has nothing to do with turbulent fluctuations. So turbulence is not what differentiates the high-*Re* regime from the medium-*Re* regime. In fact, a turbulent circular jet has the same velocity profile as a laminar one, and both spread linearly.

The cause of the anomalous rotation is still a mystery. Whatever the flow situation, the upshot must be an asymmetric distribution of shear stress on the solid surface that creates a torque. Consider a sphere placed in an eccentric position as in figure 11 but not allowed to rotate. The Coanda effect is such that the stream on the right-hand side of the sphere is faster and goes around a larger part of the circle. It is hard to imagine that the shear stress would be stronger on the left-hand side of the sphere. The flow field around an anomalously rotating sphere is shown in figure 13. There are closed streamlines around the solid surface. The stream on the left bends along the sphere and meets the stream on the right. This pattern of streamlines closely resembles that of a jet past a rotating body (Chiou & Lee 1993). Hence, it is the result of the rotation, not the cause.

In the experiments of Goldshtik (1981), cylinders and spheres that can rotate freely are inserted into the boundary of wide water and air jets. The diameter of the jet is typically a few times larger than that of the cylinder or sphere. When only one side of the solid body is in contact with the jet, it rotates normally as can be intuitively

(*a*)

(*b*)

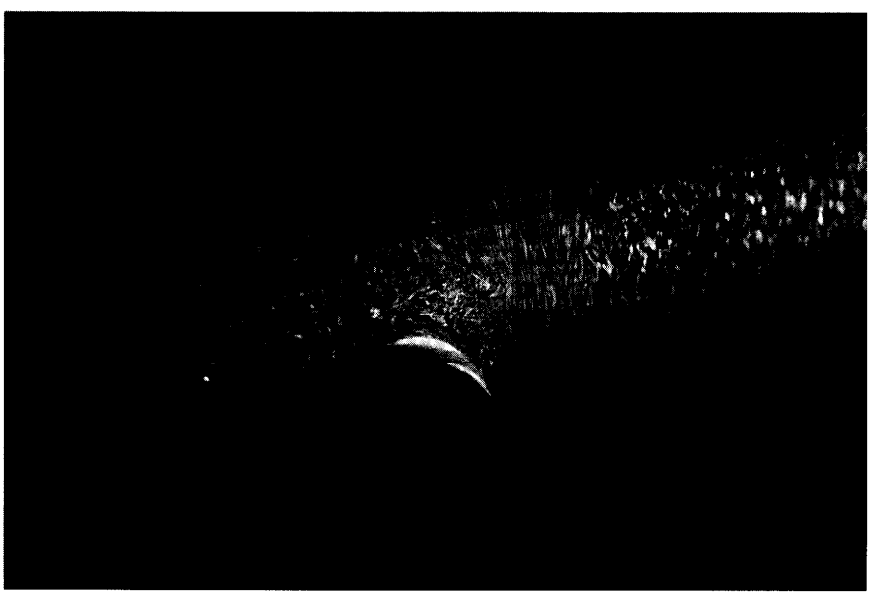

FIGURE 13. Streamlines around a rubber sphere in anomalous rotation. The laser sheet comes from the left in (*a*) and from the right in (*b*). Flow parameters are: $\rho = 1.185$, $G = 1.608 \times 10^8$, $\alpha = 10°$, $\kappa = 1$, $Re = 1.357 \times 10^4$, $(x/D, y/D) = (0.9802, 0.4657)$, $\Omega = -0.4741$.

expected. After the solid body is entirely submerged in the jet, it rotates anomalously and experiences a lateral thrust that pushes the body outwards. In our experiments we also noticed that spheres sufficiently smaller than the jet nozzle are repulsed by the jet. Hence, Goldshtik's anomalous rotation and ours may be due to the same mechanism. A fluid mechanical explanation calls for direct measurement of the flow field and

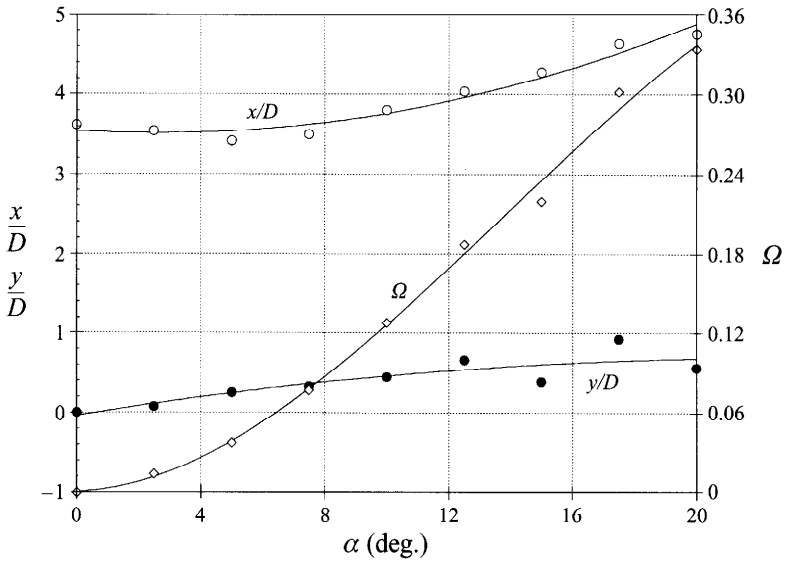

FIGURE 14. The position and rotation of an aluminium sphere in an inclined jet of polyox solution issuing from the small tube. $Re = 223.8$, $\kappa = 1.454$, $\rho = 2.755$, $G = 3.494 \times 10^3$. The Weissenberg number $We = 0.2182$.

especially the shear stress on the surface of the sphere. Numerical simulations will also be of great value. Finally, there seems to be a relationship between the rotation of the sphere and the lateral thrust on it. Anomalous rotation tends to enhance the lateral lift and reduce y/D while the opposite is true for normal rotation (figure 7). This tendency is in superficial contradiction to the Magnus effect.

3.2. *Viscoelastic jet*

Only laminar jets are studied for the polyox solution. The Reynolds number is in the hundreds. To estimate the relaxation time of the fluid λ, we use the shear-wave speed measured by Liu & Joseph (1993) for 0.85 wt% polyox solution ($c = 12.2$ cm s^{-1}) and the viscosity ν at the characteristic shear rate: $\lambda = \nu/c^2$. Then a Weissenberg number We can be calculated based on this relaxation time and the diameter of the spheres. Stable suspension was achieved with various combinations of spheres and nozzles within ranges of Re and α. Normal rotation occurs in all cases as long as the jet is inclined. The effects of α on (x, y) and Ω are shown in figure 14, in which Re and G are computed using the viscosity at the characteristic shear rate. The trends are similar to observations of turbulent Newtonian jets: x, y and Ω all increase with α. The rotation is depicted in figure 15 as a function of Re for different spheres and nozzles at a fixed inclination $\alpha = 10°$. In most cases Ω decreases as Re increases. For the small nozzle, larger spheres rotate faster (figure 15*a*, *b*). For the medium nozzle, rotation is generally much slower and the smaller sphere rotates faster than the larger one (figure 15*c*). It is not clear how viscoelastic parameters such as the Weissenberg number and the shear-thinning power-index enter the picture, so we will not write empirical correlations for the angular velocity.

The stable suspension of spheres in this Re-range provides an interesting contrast to the Newtonian experiments in the same Re-range. Note that the sphere, nozzle and Re in figure 15(*c*) are the same as in the 'unsuccessful' runs using 88% glycerol (§3.1.2). To explain this contrast, one must understand (i) how non-Newtonian properties such as shear-thinning and normal stresses affect the flow of a submerged laminar jet, and

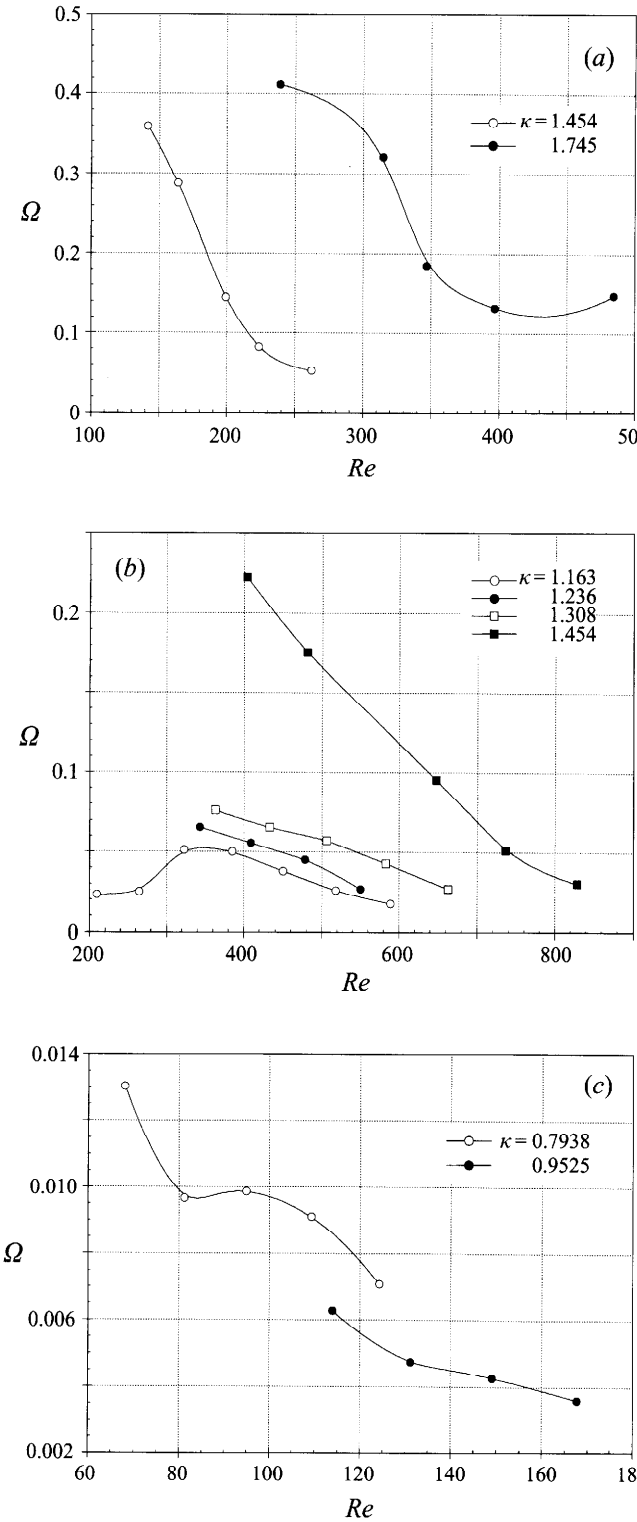

FIGURE 15. The normal rotation of spheres in the polyox solution as a function of the Reynolds number. $\alpha = 10°$. (*a*) Aluminium spheres with the small tube ($D = 1.092$ cm), $\rho = 2.755$. The parameter G is inapplicable because of the variable viscosity. $We = 0.17 \sim 0.23$. (*b*) Stainless steel spheres with the small tube, $\rho = 7.942$. $We = 0.29 \sim 0.43$. (*c*) Aluminium spheres with the medium tube ($D = 2$ cm), $\rho = 2.755$. $We = 0.19 \sim 0.25$.

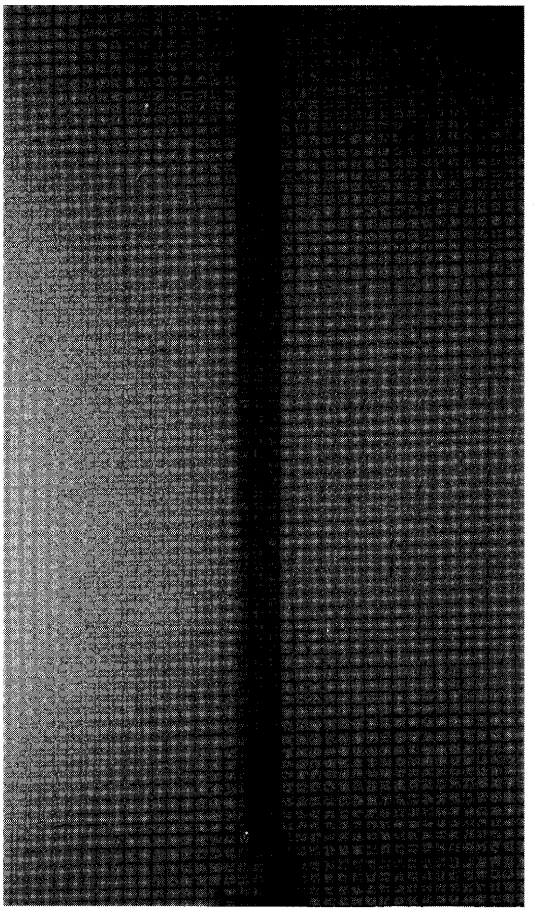

FIGURE 16. A submerged laminar jet of the polymer solution. There is little spread in the mainstream of the jet and almost no mixing along the edge. The Reynolds number based on the diameter of the nozzle and the viscosity of the liquid at the characteristic shear rate is 180.5.

(ii) in this flow field, how a viscoelastic liquid reacts to the presence of the solid sphere. A sizable literature exists on laminar pseudoplastic jets (see, for example, Mitwally 1978). Analytical and numerical studies of plane and axisymmetric jets of power-law fluids have all arrived at the same conclusion: pseudoplastic jets spread wider; the central part of the velocity profile is flatter and the maximum velocity decays faster. Jordan, Rankin & Sridhar (1992) used LDV to measure the velocity profiles at various longitudinal stations. The velocity distribution is indeed flatter in the middle, but the spread of the jet seems to be suppressed and the decay of the maximum velocity is slower. The discrepancy probably stems from the fact that the polyacrylamide solution (made from Separan AP30) retains some elasticity even after the severe agitation described in their paper.

Studies of submerged laminar viscoelastic jets are scarce. Berman & Tan (1985) intended to investigate the turbulent structure of polymeric jets. For one of their samples, 100 p.p.m. polyacrylamide in de-ionized water, the jet stays laminar for $2400 < Re < 4200$. Measurements show that this jet is narrower than a Newtonian jet at the same Re and the central velocity decay is slower, consistent with results of Jordan *et al.* (1992). In our experiments, visual observations of the tiny air bubbles in the

solution suggest that the jet entrains much less surrounding liquid than a Newtonian jet does. There is little spread in the central part of the jet (figure 16). One may also note the onset of sinusoidal instability on the top of the jet in figure 16, which resembles Berman & Tan's pictures. Hence, it can be stated that the viscoelastic jet has a narrower and steeper shear layer, owing to the elasticity of the polymer.

If a solid sphere is placed inside this shear layer, certain distributions of shear and normal stresses will develop on the solid surface which give rise to the stable suspension. No information about this process is available. The normal rotation of the sphere seems to be a direct result of the local shear. For parallel non-uniform shear flows, Ho & Leal (1976) have demonstrated that non-Newtonian normal stress causes a small sphere to migrate in the direction of decreasing shear rate. If this argument applies to the jet flow, it implies a lateral thrust toward the centre of the jet. Unfortunately, we do not know to what extent this argument applies. The role of the special attributes of a jet that a parallel shear flow does not possess cannot be assessed based on our current knowledge.

In our device, Reynolds numbers as low as 10 or as high as 10^4 cannot be realized for the polyox solution. But one is tempted to speculate on the behaviour of the ball in those two cases. In almost all flow situations involving solid particles, Newtonian and viscoelastic liquids give exactly opposite results. Quite likely, stable suspension by entrained flow is impossible at low Re, since a viscoelastic jet entrains less liquid. It is not immediately clear what behaviour to expect at high Re to complete the perfect complementarity between Newtonian and viscoelastic jets.

For the slow sedimentation of a long particle in a viscoelastic liquid, Feng *et al.* (1995) proved that the non-Newtonian normal stresses cause a reversal of the pressure distribution on the particle which explains the equilibrium orientation of the particle. We believe this mechanism is generic and is responsible for an array of 'anomalous' effects observed in the motion of particles in viscoelastic fluids. Specifically, it produces the lateral force that pulls a ball toward the centre of a viscoelastic jet at intermediate Reynolds numbers. Under similar conditions, a Newtonian jet exerts a repulsive force.

4. Concluding remarks

The experimental results discussed in the last section can be summarized as follows:

(i) A solid sphere can be suspended outside the mainstream of a laminar Newtonian jet at $Re \sim 10$. The cause of this phenomenon is the flow of surrounding fluid entrained by the jet.

(ii) At Reynolds number in the hundreds, a laminar Newtonian jet cannot suspend a solid sphere.

(iii) At high Reynolds numbers ($Re \sim 10^4$), a turbulent Newtonian jet suspends a sphere by the Coanda effect unless the sphere is too small. The rotation of the sphere in an inclined jet can be in either direction. The mechanism of the anomalous rotation is unclear.

(iv) A viscoelastic laminar jet does not spread as much as a comparable Newtonian jet; it entrains less fluid and the central velocity decays more slowly.

(v) A viscoelastic laminar jet can suspend solid spheres when the Reynolds number is in the hundreds. The lateral lift may be associated with non-Newtonian normal stresses. The rotation is always normal.

This work emphasizes observations of qualitative behaviour rather than accurate measurements, and is only a preliminary study. Fundamental data, such as the velocity field in the jet, need to be obtained from more refined experiments. Detailed

measurements of this kind may also help explain the anomalous behaviour found in our observations.

This work was supported by the NSF, Fluid, Particulate and Hydraulic Systems, by the US Army, Mathematics and AHPCRC and by the DOE, Department of Basic Energy Sciences. We are deeply indebted to our colleagues, R. Bai, A. Huang, J. Liu and C. Luo, who offered generous help with many aspects of the project. We also thank Professors M. A. Goldshtik and Y. Khavkin for stimulating discussions and suggestions. J.F. was partly supported by a Doctoral Dissertation Fellowship from the Graduate School, University of Minnesota.

REFERENCES

BERMAN, N. S. & TAN, H. 1985 Two-component laser Doppler velocimeter studies of submerged jets of dilute polymer solutions. *AIChE J.* **31**, 208–215.

BRADSHAW, P. 1973 Effects of streamline curvature on turbulent flow. *AGARDograph* No. 169.

CHIOU, C. C. & LEE, S. L. 1993 Forced convection on a rotating cylinder with an incident air jet. *Intl J. Heat Mass Transfer* **36**, 3841–3850.

FENG, J., JOSEPH, D. D., GLOWINSKI, R. & PAN, T. W. 1995 A three-dimensional computation of the force and torque on an ellipsoid settling slowly through a viscoelastic fluid. *J. Fluid Mech.* **283**, 1–16.

GOLDSHTIK, M. A. 1981 *Vortex Flows* (in Russian). Novosibirsk: Nauka.

GOLDSHTIK, M. A. 1990 Viscous-flow paradoxes. *Ann. Rev. Fluid Mech.* **22**, 441–472.

HO, B. P. & LEAL, L. G. 1976 Migration of rigid spheres in a two-dimensional unidirectional shear flow of a second-order fluid. *J. Fluid Mech.* **76**, 783–799.

JORDAN, C., RANKIN, G. W. & SRIDHAR, K. 1992 A study of submerged pseudoplastic jets. *J. Non-Newtonian Fluid Mech.* **41**, 323–337.

LIGHTHILL, M. J. 1945 Notes on the deflection of jets by insertion of curved surfaces, and on the design of bends in wind tunnels. *Aero. Res. Counc. R. & M.* 2105.

LIU, Y. J. & JOSEPH, D. D. 1993 Sedimentation of particles in polymer solutions. *J. Fluid Mech.* **255**, 565–595.

MCNAUGHTON, K. J. & SINCLAIR, C. G. 1996 Submerged jets in a short cylindrical flow vessels. *J. Fluid Mech.* **25**, 367–375.

MITWALLY, E. M. 1978 Solutions of laminar jet flow problems for non-Newtonian power-law fluids. *Trans. ASME J. Fluids Engng* **100**, 363–366.

MORRIS, P. J. 1976 The spatial viscous instability of axisymmetric jets. *J. Fluid Mech.* **77**, 511–529.

NEWMAN, B. G. 1961 The deflection of plane jets by adjacent boundaries-Coanda effect. In *Boundary Layer and Flow Control* (ed. G. V. Lachmann), vol. 1, pp. 232–264. Pergamon.

REYNOLDS, O. 1870 On the suspension of a ball by a jet of water. *Proc. Manchester Lit. Phil. Soc.* **9**, 115–120.

SCHLICHTING, H. 1979 *Boundary Layer Theory*. McGraw-Hill.

VAN DYKE, M. 1982 *An Album of Fluid Motion*. Parabolic.

WILLE, R. & FERNHOLZ, H. 1965 Report on the first European Mechanics Colloquium, on the Coanda effect. *J. Fluid Mech.* **23**, 801–819.